

Unambiguous Identification of β -Tubulin as the Direct Cellular Target Responsible for the Cytotoxicity of Chalcone by Photoaffinity Labeling

Bo Zhou⁺,^[a] Xingxin Yu⁺,^[a, b] Chunlin Zhuang,^{*[a, c]} Peter Villalta,^[d] Yong Lin,^[e] Junxuan Lu,^[f] and Chengguo Xing^{*[a]}

Chalcone is a simple and potentially privileged structure in medicinal chemistry with a diverse repertoire of biological activities, among which cytotoxicity is of particular interest. The sharp structure–activity relationship (SAR) for chalcone's cytotoxicity suggests structure-specific target interactions. Despite the numerous putative targets proposed, evidence for direct target interactions in cells is unavailable. In this study, guided by the sharp cytotoxic SAR, we developed a cytotoxic chalcone-based photoaffinity labeling (PAL) probe, (*E*)-3-(3-azidophenyl)-1-[3,5-dimethoxy-4-(prop-2-yn-1-yloxy)phenyl]-2-methylprop-2-en-1-one (C95; IC_{50} : $0.38 \pm 0.01 \mu\text{M}$), along with two

structurally similar non-cytotoxic probes. These probes were used to search for the direct cellular target responsible for chalcone's cytotoxicity through intact cell-based PAL experiments, in which β -tubulin was identified to specifically interact with the cytotoxic probe (i.e., C95) but not the non-cytotoxic probes. A set of phenotypical and biochemical assays further reinforced β -tubulin as the cytotoxic target of chalcones. Peptide mass quantitation by mass spectrometric analysis revealed one peptide potentially labeled by C95, providing information on chalcone's binding site on β -tubulin.

Introduction

Chalcone is the core structure of many natural and synthetic compounds that have demonstrated a wide range of biological activities, including anticancer, anti-inflammatory, antioxidative, and antibacterial activities.^[1] Quite a number of proteins and

related mechanisms have been reported that may account for chalcone's diverse biological activities.^[2] These results, however, also raise the question as to whether the chalcone template is a privileged structure or a promiscuous one, particularly given its potential to function as a Michael acceptor that may react nonselectively with nucleophiles on various biological molecules. Among the reported biological activities, chalcone's anticancer potential has been studied extensively, and many lead compounds have been identified, including a number of natural products such as isoliquiritigenin, xanthohumol, and licochalcone A.^[3] Chalcone's anticancer potential is particularly interesting, because the cytotoxicity is highly structure dependent, with potency ranging from low nanomolar to high micromolar even among chalcones of minimal structural differences (Figure 1).^[4] Such sharp structure–activity relationships (SAR) suggest a well-defined and critical interaction of the cytotoxic chalcone with its responsible cellular target(s), which supports chalcone as a privileged structure.^[4c,5] Nevertheless, mechanistic studies to date have identified many putative cellular targets that may account for chalcone's cytotoxicity, including tubulin,^[6] kinases,^[7] cathepsins,^[8] topoisomerases,^[8b,9] MDM2,^[10] and many others.^[11] The relevance and contribution of these potential drug–target interactions to chalcone's cytotoxicity are not well characterized. Moreover, there has been little evidence to support any direct interactions of cytotoxic chalcones with these putative targets in intact cells. Taking tubulin as an example, although chalcone-based compounds have been documented to inhibit tubulin polymerization *ex vitro*,^[6c,e] their direct interaction in cells remains to be validated. Similarly, whereas cells upon cytotoxic chalcone exposure would lose

[a] Dr. B. Zhou,⁺ Prof. X. Yu,⁺ Dr. C. Zhuang, Prof. C. Xing
Department of Medicinal Chemistry, College of Pharmacy,
University of Minnesota, 2231 6th Street SE, Minneapolis, MN 55455 (USA)
E-mail: xingx009@umn.edu
zhuan092@gmail.com

[b] Prof. X. Yu⁺
Shanghai Key Laboratory of New Drug Design, School of Pharmacy,
East China University of Science and Technology, Shanghai 200237 (China)

[c] Dr. C. Zhuang
Research Center for Marine Drugs, School of Pharmacy,
Second Military Medical University,
325 Guohe Road, Shanghai 200433 (China)

[d] Dr. P. Villalta
Masonic Cancer Center, University of Minnesota,
2231 6th Street SE, Minneapolis, MN 55455 (USA)

[e] Prof. Y. Lin
Molecular Biology and Lung Cancer Program,
Lovelace Respiratory Research Institute, Albuquerque, NM 87108 (USA)

[f] Prof. J. Lu
Department of Pharmacology and Cancer Institute,
Penn State University College of Medicine, Hershey, PA 17033 (USA)

[†] These authors contributed equally to this work.

Supporting Information (detailed procedures for probe syntheses and their chemical characterization, protocol for cytotoxicity assays, biotin–streptavidin-based western blot analysis of the cytoplasmic fractions, additional data of MS analysis and target identification, and target validation results by anti- β -tubulin western blot and tubulin polymerization assays) and the ORCID identification number(s) for the author(s) of this article can be found under <http://dx.doi.org/10.1002/cmdc.201600150>.

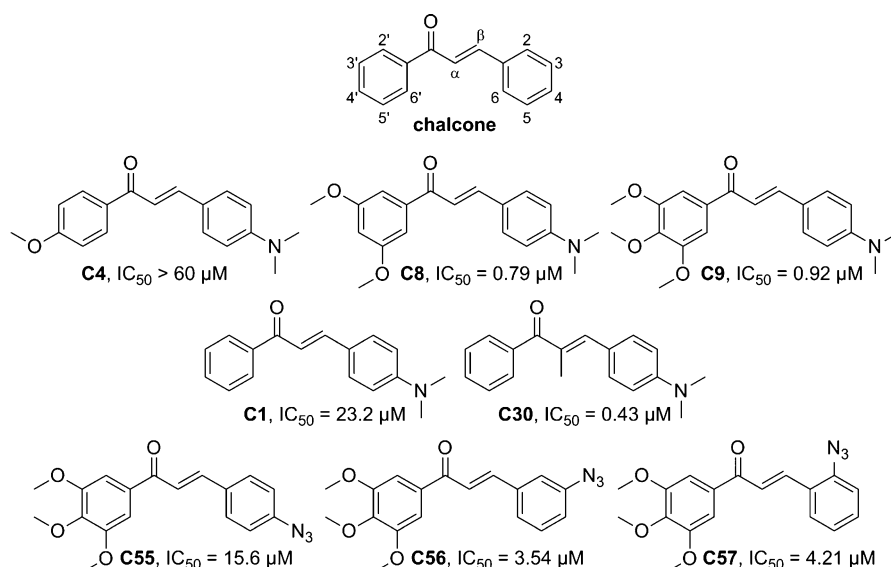


Figure 1. Chalcone's structural scaffold and examples of chalcones with a sharp SAR on cytotoxicity that is critical to the design of PAL probes.

microtubule structure, such an effect can be mediated by multiple mechanisms.^[12] Therefore, there is a critical need to characterize the direct chalcone–target interaction in cells that are responsible for chalcone's cytotoxicity. Such knowledge will help to guide future rational optimization and translational development of chalcone-based anticancer candidates.

Various approaches have been developed to identify the direct cellular targets of drug candidates. The photoaffinity labeling (PAL) approach is of particular importance, because of its ability to capture direct drug–target interactions through the formation of a covalent bond upon UV exposure (Figure 2A). Facile target identification is usually achieved by link-

ing the on-target PAL probe to a fluorescent or biotin functional group through synthetic methods, such as the click reaction, for target visualization or enrichment. This approach, if applied to the intact cell system, can, to a great extent, unbiasedly reveal the direct cellular target profile of the drug candidate under physiologically relevant biological conditions.^[13]

To the best of our knowledge, no chalcone-based PAL probes have been explored for the identification of chalcone's direct cellular targets. In this study, we employed this approach to search for the cellular targets responsible for the cytotoxicity of chalcone. Three chalcone-based PAL probes (i.e., C90, C91, and C95; Figure 2B) with similar structures yet with dis-

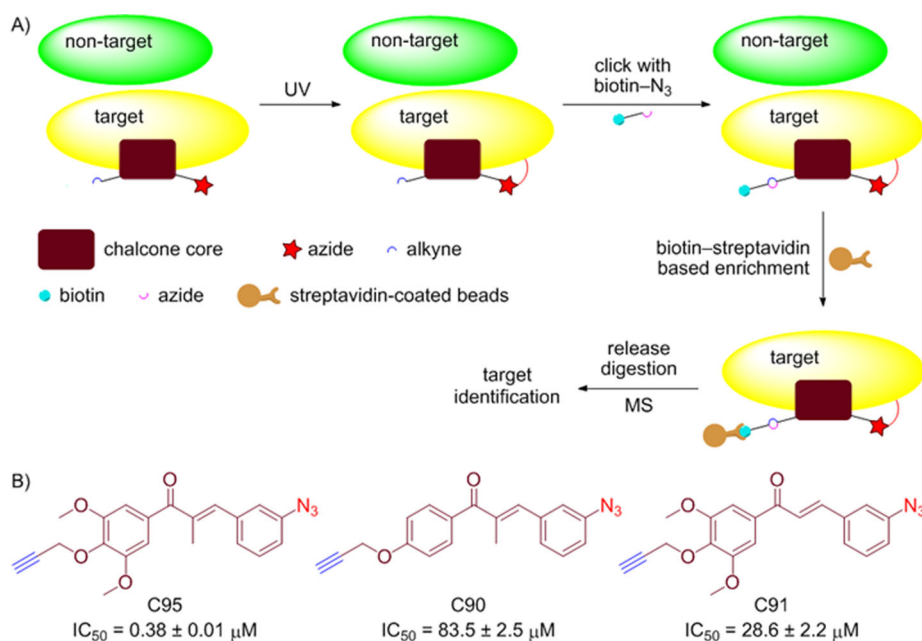


Figure 2. Design of chalcone-based PAL probes for cytotoxicity target investigation. A) Scheme of target protein labeling, enrichment, and MS identification with chalcone-based PAL probes. B) Structures of the chalcone-based PAL probes and their cytotoxicity IC_{50} values against A549 cells.

tinct cytotoxicity were developed. Cell-based PAL experiments revealed clear and distinct target protein labeling patterns among these three probes, which suggested that these chalcones have a high level of discrimination in the cellular proteome. Interestingly, one 52 kDa protein was selectively labeled by C95, the cytotoxic PAL probe, but not by the non-cytotoxic probes. Competition with cytotoxic and non-cytotoxic chalcones lacking the PAL functional groups further supported this protein as the target responsible for chalcone's cytotoxicity. Subsequent streptavidin–biotin-based target enrichment and mass spectrometry (MS) analysis unambiguously identified the target protein as β -tubulin, which was further supported by a number of biochemical and phenotypical assays. Our MS analysis also revealed the potential binding site for chalcones on β -tubulin. These data are valuable for the understanding and future optimization of chalcone's cytotoxicity. The success also demonstrates the feasibility of PAL as a general approach to explore the cellular targets responsible for the diverse bioactivities of chalcone. Lastly, the results herein provide compelling evidence supporting that chalcone can be developed as a privileged structure instead of a promiscuous one.

Results and Discussion

Design, syntheses, and cytotoxicity-based selection of positive and negative PAL probes

We previously synthesized a library of chalcone compounds and determined their cytotoxicity against A549, a human non-small-cell lung adenocarcinoma cancer cell line.^[4] Those compounds showed a sharp SAR, with IC_{50} values ranging from sub-micromolar to $>60 \mu\text{M}$ (Figure 1). We found that methoxy groups at the 3',5'-positions greatly favored the cytotoxic potency, whereas a small-sized functional group at the 4'-position did not have much impact. An azido substituent was well tolerated at the 3-position but was less tolerated at the 2- and 4-positions, particularly the 4-position. A methyl substituent at the α -alkenyl carbon atom was found to significantly increase the cytotoxic potency. These SAR results guided the design of the structurally similar cytotoxic and non-cytotoxic PAL probes—C90, C91, and C95 (Figure 2B). The non-cytotoxic PAL probe(s) were expected to serve as controls to help discriminate the cellular targets—whether they would be responsible for chalcone's cytotoxicity. Among the three probes, an azido functional group was introduced at the 3-position as the PAL group, whereas a propargyl ether linkage was introduced at the 4'-position as the handle, as illustrated in Figure 2A. Methoxy groups were designed at the 3',5'-positions of C95 with a methyl substitution at the α -alkenyl carbon atom to maximize its cytotoxicity potency. The non-cytotoxic probes, C90 and C91, lacked either the methoxy groups at the 3',5'-positions or the α -alkenyl methyl group. The synthetic scheme (Scheme S1) and detailed procedures are provided in the Supporting Information. These three probes were first evaluated for their cytotoxicity against A549 cells following our established procedures.^[4c] As expected, C95 had a sub-micromolar IC_{50} ($0.38 \pm 0.01 \mu\text{M}$) value to inhibit the proliferation of A549

cells, which served as the positive PAL probe. C90 [$IC_{50} = (83.5 \pm 2.5) \mu\text{M}$] and C91 [$IC_{50} = (28.6 \pm 2.2) \mu\text{M}$] were >200 - and 75-fold less potent, which served as the control probes.

Intact cell-based proteome profiling with the PAL probes

To unbiasedly capture the drug–target direct interactions of our PAL probes in the cellular environment, we performed intact cell-based photoaffinity labeling experiments. Briefly, A549 cells were pretreated with the PAL probes, which was followed by covalent bond formation between the PAL probe and its cellular target(s) upon UV activation of the azido functional group. Cells were lysed, and the lysates were subjected to the click reaction through the propargyl functional group on the PAL probe with an azido-functionalized biotin [Figure S1, biotin–PEG– N_3] so that the PAL-probe-labeled target(s) were selectively tagged with a biotin modification. Such lysates were then resolved by SDS-PAGE, followed by streptavidin-based western blotting to visualize the biotinylated proteins. The results (Figure 3A) showed that these three probes had distinct labeling patterns; C91 barely labeled any proteins, whereas C90 labeled dominantly one protein at ~ 55 kDa and slightly another protein at ~ 36 kDa. The cytotoxic probe, C95, dose-dependently labeled mostly three proteins (~ 36 , ~ 52 , and ~ 55 kDa), particularly if its concentration was at 0.5 or $1 \mu\text{M}$, which is close to its cytotoxic IC_{50} value. Among these three proteins, C95 preferentially labeled the one at 52 kDa (red arrow in Figure 3A). The different labeling patterns among the three PAL probes in the cellular proteome suggest that they have distinct and highly selective cellular target profiles. In addition, the absence of any protein labeling by C95 without UV activation (the last lane in Figure 3A) indicated a noncovalent nature of the interactions between C95 and its cellular targets, despite its α,β -unsaturated ketone functional group as a potential Michael acceptor.^[14] The distinct labeling profiles of structurally very similar probes support that the chalcone core structure in these probes is likely a privileged structure.

More interestingly, the protein at 52 kDa was only labeled by the cytotoxic probe and not by either of the two non-cytotoxic probes. These data suggest that this 52 kDa protein may be the direct target responsible for chalcone's cytotoxicity. To further explore this, a set of competitive labeling experiments were performed (Figure 3B).^[15] In brief, A549 cells were co-treated with C95 and either cytotoxic chalcone C8 ($IC_{50} = 0.79 \mu\text{M}$) or non-cytotoxic chalcone C4 ($IC_{50} > 60 \mu\text{M}$), both of which are structurally similar to C95 but do not possess the PAL group (Figure 1), and this was followed by the standard photoaffinity labeling procedures. The results (Figure 3B, red arrow) showed that cytotoxic C8 significantly decreased the extent of labeling of the 52 kDa protein by C95 with no significant competing effects on the other two proteins. Non-cytotoxic C4, on the other hand, decreased the extent of labeling of the proteins at 36 and 55 kDa by C95 with no competing effect on the 52 kDa protein. These data provide additional evidence that suggest that the 52 kDa protein is chalcone's direct cellular target responsible for its cytotoxicity.

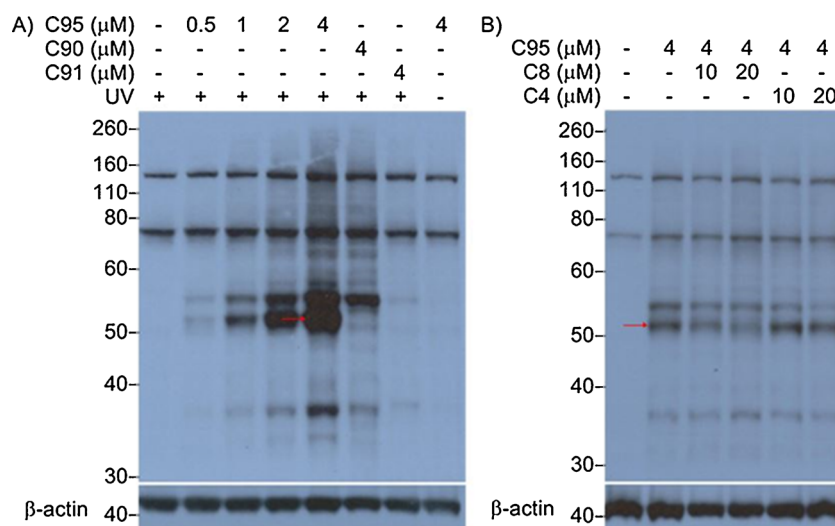


Figure 3. Intact cell-based photoaffinity labeling of the cellular target proteins by the cytotoxic and non-cytotoxic PAL probes. A) Dose–response photoaffinity labeling of the cellular proteins with cytotoxic probe C95 in comparison with non-cytotoxic probes C90 and C91 and the necessity of UV activation for covalent labeling. B) Differential competition of C95-labeled cellular proteins with cytotoxic chalcone C8 and non-cytotoxic chalcone C4.

Subcellular fractionation-based and biotin–streptavidin-based enrichment of C90- and C95-labeled target proteins

Given that probe C91 showed minimal labeling in the intact cell-based target profiling, C90 was selected as the control probe to C95 for latter studies. To isolate the target proteins for MS-based analysis, we first attempted target enrichment on the basis of a standard subcellular fractionation in the hope that the target proteins would be distributed in specific subcellular fractions. A549 cells, upon PAL experiments, were lysed into four fractions by using a commercial kit: the cytoplasmic fraction (CF), the membrane fraction (MF), the nuclear fraction (NF), and the pellet fraction (PF). These four fractions were subjected to click reactions with an azido-functionalized biotin and were then analyzed by streptavidin-based western blot (Figure S2). It is clear that the majority of the PAL-probe-labeled proteins were in the cytoplasmic fraction. The membrane fraction contained only a small amount of these proteins, which might have been partly caused by crossover among the adjacent fractions. The nonspecific signals (~75 and ~150 kDa, respectively, likely as a result of endogenous biotin-modified proteins) were not detectable in the cytoplasmic fraction. Through this standard cellular fractionation, we were able to enrich the proteins selectively labeled by the PAL probes and to decrease the endogenous background significantly.

To further enrich the PAL-probe-labeled target proteins, the cytoplasmic fraction, after click reaction based selective biotin modification, was incubated with streptavidin-coated beads to separate the PAL-probe-labeled proteins from the rest of the proteome. As expected, the supernatants after probe-labeled target enrichment showed no biotin signal (Figure 4A), whereas their Coomassie blue staining patterns were indistinguishable from those of the original cytoplasmic lysates (Figure 4B). The enriched samples, upon release from the beads under de-

naturing conditions, showed a biotin signal pattern similar to that of the original lysate, whereas they showed minimal Coomassie blue staining other than the two proteins at ~55 and 52 kDa. These two proteins were not the most abundant endogenous proteins, which further supports chalcone's specific interactions with the cellular proteins. These results demonstrated that the PAL-probe-labeled proteins were efficiently and selectively enriched from the cytoplasmic fraction.

Protein target identification by mass spectrometry

The 52 kDa protein band in the C95-treated enriched sample lane was collected from the Coomassie blue stained gel (Figure 4B). The gel regions of the same molecular weight from the C90-treated and DMSO-control samples were also collected. These gel bands were subjected to in-gel trypsin digestion followed by MS analysis of the digested peptides for protein target identification. Five rounds of experiments were performed: the first three rounds were biological repeats, whereas the last two rounds had slight procedural modifications as detailed later. The MS-based peptide identification results from each round were searched against a UniProt human protein database by using Proteome Discoverer (PD). The representative data (round 3) are shown in Figure S3. The combined MS results from all five rounds revealed several isoforms of β -tubulin along with one α -tubulin isoform as the only target candidates for C95 (Figure 4C) that met the following two criteria: 1) having a PD score > 10 in every round; 2) not keratin. The PD scores and #PSM (number of peptide-spectrum match), two commonly used parameters for protein identification,^[16] of these protein hits in the C95-treated sample were also compared with those of the DMSO control sample and the C90-treated sample in each round to eliminate false positives as a result of potential nonspecific interactions. All tubulin isoforms showed significantly higher PD scores and #PSM in the

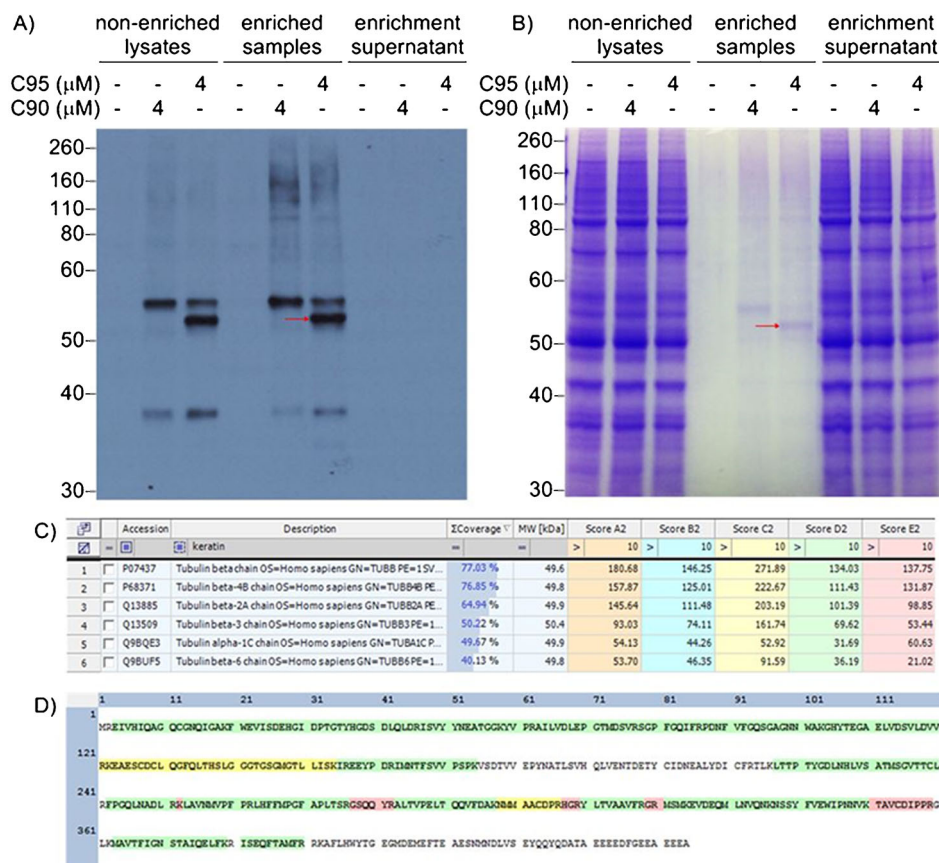


Figure 4. Enrichment and identification of PAL-probe-labeled proteins. A) Biotin–streptavidin-based western blot and B) Coomassie blue staining of cytoplasmic lysates before and after enrichment with streptavidin-coated beads. C) Combined report of protein hits identified in five rounds of MS experiment of the C95-treated sample, and D) overall coverage of TUBB from all five rounds combined. Red arrows in panels A) and B) indicate the 52 kDa protein in the enriched samples; hit filters applied for panel C) were “description does not contain ‘keratin’” and “score > 10”.

Table 1. Proteins identified as the top candidates from the PAL-probe-based intact-cell proteome labeling experiment.^[a]

Protein ID ^[a]	Protein Name ^[a]	Gene Symbol ^[a]	C95		C90		Control	
			Score	#PSM	Score	#PSM	Score	#PSM
P07437	tubulin β chain	TUBB	180.68	71	52.68	19	5.87	2
P68371	tubulin β-4B chain	TUBB4B	157.87	64	39.91	17	7.88	3
Q13885	tubulin β-2A chain	TUBB2A	145.64	59	42.06	15	3.77	1
Q13509	tubulin β-3 chain	TUBB3	93.03	40	24.60	12	5.77	3
Q9BQE3	tubulin α-1C chain	TUBA1C	54.13	23	22.65	13	11.73	5
Q9BUF5	tubulin β-6 chain	TUBB6	53.70	25	19.45	8	0	0

[a] Shown here are results from a representative round of five. Complete results of all five rounds can be found in Table S1. Protein IDs, names, and gene symbols are based on the UniProtKB database.

C95-treated sample than in the C90-treated or DMSO control samples (Table 1 for round 1 and the data for the other four rounds are in Table S1), which confirmed that they were preferentially labeled by cytotoxic C95. The one α-tubulin isoform showed a much lower PD score and #PSM than the top β-tubulin isoforms, which suggested that β-tubulin was the main protein labeled by C95, with a much weaker interaction with α-tubulin potentially through binding at a site near the dimer interface on β-tubulin such as the colchicine-binding site.^[17]

Among the β-tubulin isoforms, a high sequence coverage (77.03%) was achieved for the top hit tubulin β chain (TUBB)

(Figure 4D). The theoretical peptides from TUBB upon trypsin digestion were compared with the detected peptides, and all medium-sized theoretical peptides (5–35 residues, Table S2) were found to be unambiguously detected with high-confidence MS² spectra in the C95 sample. Lastly, anti-β-tubulin western blotting was performed, and it confirmed the presence of β-tubulin in the enriched C95-treated cell samples, which was absent in C90-treated samples (Figure 5). These results unambiguously identified tubulin, particularly β-tubulin, as the 52 kDa protein that selectively interacted with the cytotoxic PAL probe C95 in intact A549 cells.

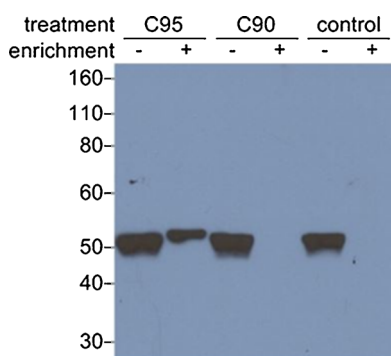


Figure 5. Target validation by anti- β -tubulin western blot of non-enriched samples (8 μ g) and streptavidin-enriched samples (from 40 μ g of non-enriched sample).

Attempts to identify C95-modified peptides on β -tubulin directly

The binding sites on the target protein(s) for the PAL probes could be preliminarily characterized by identifying PAL-probe-labeled peptides and even the specific amino acids by data mining the MS² data.^[13d,18] We first attempted to directly search for C95-modified peptides from the trypsin-digested peptide samples (rounds 1 and 2). The input for the MS² data search was based on the data of our model reaction of the UV-activated reaction of the probe (Figure S4) with theoretical modification of the azido-functionalized biotin (Figure S1, biotin-PEG-N₃). We also tried to enrich C95-modified peptides from the trypsin-digested samples by streptavidin beads followed by MS² analysis (round 3). All these attempts, however, resulted in no hits. We reasoned that the lack of success might have been caused by the large hydrophobic probe-biotin functional group, which might have significantly changed the properties of the modified peptide(s) and prevented their recovery from PAGE or the C₁₈ column (C₁₈ column was used for desalting before MS analysis). The probe-biotin modification may have also compromised the ionization of the modified peptide or MS² fragmentation. We therefore modified the experimental protocol to remove the desalting step and acquired the MS² data with the collision-induced dissociation (CID) fragmentation mode (round 4). This attempt also did not lead to any potential hits.

We then employed an UV-cleavable biotin azide (Figure S1), wishing to optimize the properties of the C95-modified peptide(s) (round 5). The labeled cytoplasmic lysates were subjected to click reaction with the UV-cleavable biotin azide, followed by enrichment, in-solution digestion, beads capture, and UV cleavage of the labeled peptides. Again, the experimental conditions were optimized by using our model compound, and MS search was based on the MS fragmentation of the model compound (Figure S5). Disappointingly, this attempt also did not identify any modified peptides with an unambiguous MS² spectrum.

Indirect identification of the C95-modified peptide on β -tubulin by quantifying the abundance of unmodified peptides

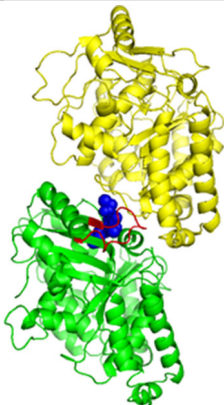
We then resorted to using MS-based peptide quantitation as an indirect approach to search for probe-modified peptides. Our rationale was that if a trypsin-digested peptide from β -tubulin was modified by C95, which was not detected in our previous attempts, the relative abundance of this natural peptide detected should then decrease. The data analysis was performed by following the reported label-free MS quantitation method.^[15,19] Briefly, the extracted ion chromatograms (EIC) of the peptides with high-confidence MS² spectra were obtained from the full MS¹ chromatograms. The peak areas of the same peptide among the different samples in the same experiment were integrated and compared in order to determine the relative abundance of such a peptide in the samples. Trypsin peptides resulting from autolysis were analyzed as quality controls for quantitation, as they should have equal abundance in all the samples within the same experiment. As shown in Table S3, four unique peptides derived from trypsin consistently showed similar abundances in C95-, C90-, and DMSO-treated samples, and this established the feasibility and reliability of this quantification method. Given that TUBB was the top hit among the tubulin isoforms, peptides of TUBB detected in rounds 1–3 were analyzed. Rounds 1–3 were used for analysis because they were performed under the same conditions. The ratios of the abundance of the TUBB peptides in the C95-treated samples to that in the DMSO control samples were calculated (Table 2). Among the 14 peptides detected, the ratio of peptide N337K350 (NSSYFVEWIPNNVK) was the only one that was out of the 99% confidence interval in all three rounds of experiments. The ratio was also the lowest among the 14 peptides in each round. The unusually low ratio of this peptide in C95 to control samples suggested that C95 likely modified this peptide, which led to a decrease in the amount of its natural form. A close inspection of the X-ray structure of a colchicine-tubulin heterodimer complex^[17] revealed that the terminal lysine residue of this peptide resides in the colchicine binding site, which suggests that the binding site of C95 on tubulin may overlap with the colchicine binding site (embedded figure in Table 2). This potential binding site is consistent with several other literature reports. For instance, docking studies suggested that cytotoxic chalcones fit well in the colchicine binding site,^[20] and colchicine was shown to compete with cytotoxic chalcones for tubulin binding.^[6c] Such a potential binding site is also consistent with the fact that C95 labeled α -tubulin as well, which indicated that C95 may bind around the interface of the α -tubulin and β -tubulin heterodimer.

Additional results that support β -tubulin as the direct responsible cellular target of cytotoxic chalcones

To further investigate whether β -tubulin was the target responsible for chalcone's cytotoxicity, we first evaluated the effect of C95 on tubulin polymerization by following the standard microtubule formation assay (see details in the Supporting Information).^[6c] C95 (3 μ M) significantly inhibited microtubule for-

Table 2. MS-based quantitative analysis^[a] of the natural peptides from TUBB in rounds 1–3, which were performed under the same conditions. Data in the row highlighted in red pertain to the structure on the right (produced from PDB ID: 1SA0), which shows the structural relationship among α -tubulin (yellow), β -tubulin (green), the potential labeled peptide (red), and the colchicine (blue) binding site on β -tubulin.

Peptide	C95/Ctrl Ratio		
	Round 1	Round 2	Round 3
Y310-R318	44	51	105
F242-R251	36	38	104
L253-R262	20	38	179
I381-R390	47	37	162
I47-K58	109	50	87
I163-K174	24	92	179
E325-K336	44	42	63
A63-R77	25	44	130
A283-K297	58	59	82
N337-K350	6	8	16
G104-R121	27	35	64
L217-R241	39	58	42
S78-K103	22	34	39
F20-R46	41	36	95
average^[b]	39 ± 20	44 ± 15	96 ± 41



[a] Parameters for quantitation: mass tolerance 10 ppm, Gaussian peak smoothing at 5 points; only peaks integrated > 50000 in all samples in all three rounds were analyzed. [b] Averages are given as the mean values of all of the analyzed peptides with 99% confidence interval.

mation, whereas C90 and C91 at the same concentration had much weaker inhibitory effects (Figure S6). These results are highly consistent with our earlier work, which showed that cytotoxic chalcones induce microtubule depolymerization in cells (manuscript under review). G_2/M -phase cell-cycle arrest is another key feature of anti-microtubule-agent-introduced cytotoxicity.^[6c,21] We previously showed that cytotoxic chalcone C8 arrested A549 cells at the M phase in dose- and time-dependent manners, whereas nontoxic chalcone C4 did not affect cell cycle (manuscript under review). Consistently, C95 at a concentration of 0.5 μM , similar to its IC_{50} , effectively arrested A549 cells at the G_2/M phase, whereas neither of the two non-cytotoxic probes showed any effect on the cell-cycle distribution under the same treatment conditions (Figure S7). Interestingly, even at concentrations similar to their own IC_{50} values, non-cytotoxic probes C90 and C91 did not cause significant changes in cell-cycle populations (the last two bars in Figure S7). These results suggest that tubulin is likely the responsible cellular target only for the cytotoxic chalcones but not for the non-cytotoxic chalcones. Finally, C95 was evaluated against a panel of human cancer cell lines through the NCI-60 screening service (Figure S8). C95 had an average IC_{50} value of 0.26 μM , which is similar to its IC_{50} value in A549 cells determined in our studies (0.38 μM). C95 also showed varied potencies among the screened cancer cell lines (IC_{50} ranging from 26.9 nM to 28.8 μM). C95 was then analyzed against other compounds that were evaluated through the same NCI service by COMPARE and CellMiner for their cytotoxicity potency fingerprint similarity.^[22] Ten antimitotic agents showed a correlation of > 0.5 with C95, which suggested a similar mechanism

Table 3. Top candidates that have high correlation with C95 by CellMiner/COMPARE analysis of their cytotoxic potency among the NCI-60 human cancer cell lines.

Antimitotic Agent	Correlation ^[a]
rhizoxin	0.647 ^[b]
nakiterpiosin	0.641 ^[c]
estramustine	0.628 ^[c]
desacetylcolchicine D-tartrate	0.578 ^[b]
S-trityl-L-cysteine	0.569 ^[b]
(-)-dactyloide	0.532 ^[c]
fenbendazole	0.516 ^[c]
colchicine	0.507 ^[b]
mebendazole	0.504 ^[c]
N-benzoyl deacetylcolchicine	0.501 ^[b]

[a] Correlation with C95 was calculated by using both CellMiner and COMPARE services, with the higher value reported. [b] Correlation by COMPARE. [c] Correlation by CellMiner.

of cytotoxicity (Table 3). Except for S-trityl-L-cysteine and estramustine, the other eight compounds were all shown to exert their antimitotic activity through direct interactions with tubulin.^[6c,23] Taken together, these results further support that β -tubulin is the direct cytotoxic cellular target for C95 and provide a mechanistic pathway—cytotoxic chalcones function as anti-microtubule agents by directly binding to β -tubulin around the colchicine binding site; such a binding interaction inhibits tubulin polymerization and disrupts tubulin–microtubule dynamics; this results in cell-cycle arrest at the G_2/M phase and finally leads to cell death.

Conclusions

We developed three chalcone-based photoaffinity labeling (PAL) probes to characterize the direct interaction of chalcone with its cellular targets, particularly the target(s) responsible for its cytotoxicity. By integrating the photoaffinity labeling approach with other techniques, the results herein provided compelling evidence that cytotoxic chalcones directly interact with β -tubulin in cells, which leads to the disruption of cellular microtubule dynamics and consequently cell-cycle arrest at the G_2/M phase. Although tubulin and a list of other proteins were previously suggested to be involved in the cytotoxicity of chalcone, this work demonstrated direct chalcone–tubulin interaction in intact cells and the critical role of such an interaction in chalcone's cytotoxicity. The knowledge with respect to the binding site on tubulin deserves further investigation, and this will provide structural information to explain the sharp structure–activity relationship and to guide further optimization of chalcone-based anti-microtubule agents. The PAL methodology employed herein can also be explored to search for the cellular targets that are responsible for the other biological activities of chalcone. Lastly, the high target selectivity of the three chalcones in intact cells and their sharp SARs in cytotoxicity suggest that chalcone can be developed as a privileged structure for medicinal chemistry and chemical biology. Altogether, such mechanistic knowledge of the direct cellular target interaction responsible for chalcone's cytotoxicity revealed in this

study is critical for future rational optimization and translational development of chalcone-based compounds as potential anticancer agents.

Experimental Section

Cell line and culture conditions: Human non-small-cell lung adenocarcinoma A549 cells, from ATCC, were cultured in Dulbecco's modified Eagle medium (DMEM) with 10% fetal bovine serum (FBS), penicillin (100 U mL^{-1}), and streptomycin ($100 \mu\text{g mL}^{-1}$) at 37°C with 5% CO_2 . Cells, upon reaching 80% confluency, needed to be passaged by the standard trypsin method.

Intact cell-based photoaffinity labeling with PAL probes: A549 cells were seeded in six-well plates (2×10^5 cells per well in 2 mL medium) or 100 mm cell culture dishes (2×10^6 cells per plate in 10 mL medium) and incubated for 20–24 h for attachment. The old medium was removed and the new medium, containing the corresponding probe at the specified concentrations, was added. After 1.5 h incubation, plates or dishes were exposed to UV light by a UV illuminator (312 nm) for 8 min to activate the azide for probe–target covalent labeling. Cells were then collected by standard trypsin treatment, pelleted, and lysed with EDTA-free radioimmunoprecipitation assay (RIPA) buffer. The protein concentration of the lysates was determined by the standard BCA assay. The lysates were diluted to a final concentration of $1 \mu\text{g } \mu\text{L}^{-1}$ with phosphate-buffered saline (PBS) and were stored at -80°C until use.

Introduction of biotin to the PAL probe in the cell lysates by click chemistry: To the lysate sample (30 μL) was sequentially added azido-functionalized biotin (0.35 mM in DMSO, 3 μL), tris(2-carboxyethyl)phosphine (14 mM in H_2O , 3 μL), tris(benzyltriazolylmethyl)amine (2.8 mM in 3:1 *tert*-butyl alcohol/DMSO, 3 μL), and copper(II) sulfate (16.8 mM in H_2O , 3 μL) to reach a final concentration of 25 μM , 1 mM, 200 μM , and 1.2 mM, respectively. For the click reaction with the use of subcellular fraction lysates, which contained EDTA (1 mM), the concentration of copper(II) sulfate was increased to 2 mM to achieve optimal reaction efficiency. The mixture was incubated at room temperature for 1 h in the dark. For larger scale sample preparation, up to 500 μL of lysate was used and all reagents were proportionally adjusted.

Subcellular fractionation: A549 cells, cultured in 100 mm cell culture dishes, were treated with the PAL probes and exposed to UV light the same way as that described above. Cells were then collected by trypsin treatment and were fractionated by using a cellular fractionation kit (Thermo Scientific #78840) following the manufacturer's protocol. Briefly, the cell pellet ($\sim 10^7$ cells) was sequentially extracted with cytoplasmic extraction buffer (400 μL , 10 min at 4°C , centrifuged at 500 *g* for 5 min), membrane extraction buffer (200 μL , 10 min at 4°C , centrifuged at 3000 *g* for 5 min), nuclear extraction buffer (75 μL , 30 min at 4°C , centrifuged at 5000 *g* for 5 min), RNase-containing nuclear extraction buffer (50 μL , 5 min at 37°C , centrifuged at 17000 *g* for 5 min), and pellet extraction buffer (50 μL , 10 min at room temperature, centrifuged at 17000 *g* for 5 min). Protein concentrations in each fraction were determined following the BCA method and were then diluted to $1 \mu\text{g } \mu\text{L}^{-1}$ accordingly with PBS. Protein lysates were stored at -80°C until use.

Western blot analysis: Protein samples were resolved with the Novex NuPAGE gel electrophoresis system following the manufacturer's protocol by using commercial 4–12% SDS-PAGE gels (Invitrogen #NP0322). The proteins in the gel was transferred onto a cellulose membrane and blocked with 1% bovine serum albumin (BSA) in 0.05% Tween-20/PBS for 1 h. The membrane was washed

twice with 0.05% Tween/PBS, then incubated with streptavidin–horseradish peroxidase (HRP) conjugate (1:5000, BioLegend #405210) in 0.05% Tween/PBS for 1 h. For anti- β -tubulin experiments, membrane was blocked with 5% BSA in 0.1% Tween-20/TBS for 1 h and then incubated with HRP-conjugated β -tubulin antibody (1:1000, Cell Signaling Technology #5346) in 0.1% Tween-20/TBS containing 5% BSA for overnight. After three washes with 0.05% Tween/PBS, the membrane was incubated in SuperSignal West Pico chemiluminescent substrate mix (Thermo Scientific #34080) for 8 min with gentle shaking. The autoradiology film (GeneMate #F-9023-5X7) was then exposed to the membrane for a suitable period (typically within 2 min) and was developed in an automatic film developer (Konica Minolta SRX-101A).

Enrichment of biotinylated PAL-probe-labeled proteins with streptavidin-coated beads: A streptavidin T1 beads slurry (67 μL , Invitrogen #65601) was washed thoroughly with PBS in a microcentrifuge tube. The beads were then incubated with the cytoplasmic fraction lysate (200 μL) with gentle rotation by using a rotary shaker (4°C , overnight). The beads were washed with 0.05% Tween-20/PBS (400 $\mu\text{L} \times 2$), 1 M NaCl in 0.1% Tween-20/PBS (400 $\mu\text{L} \times 2$), and 0.5% SDS/PBS (100 μL). The beads were then mixed with 0.5% SDS/PBS (14 μL) and heated (95°C , 5 min) to release the proteins from the beads. The protein sample was then subjected to SDS-PAGE analysis. Typically, 5% of such protein sample was used for western blot analysis, whereas the remaining sample was used for Coomassie blue staining, in-gel digestion, and MS analysis.

In-gel digestion: The SDS-PAGE gel was stained with Imperial Coomassie staining (Thermo Scientific #24615) to visualize the target proteins. The gel region corresponding to a protein molecular weight of ~ 52 kDa was cut out and diced into 1 mm cubes. To the diced gel samples was added ammonium bicarbonate (25 mM, 100 μL) and dithiothreitol (300 mM, 10 μL). The mixture was incubated for 15 min at 50°C . Then, saturated iodoacetamide (10 μL) was added, and the mixture was incubated for 15 min at room temperature. The supernatant was removed, and the gel pieces were washed with a mixture of 1:1 v/v acetonitrile/25 mM ammonium bicarbonate (100 $\mu\text{L} \times 2$) and acetonitrile (100 μL). The residual solvent was removed by speed-vac, and the gel pieces were resuspended in ammonium bicarbonate (25 mM, 75 μL); trypsin (0.1 $\mu\text{g } \mu\text{L}^{-1}$, 25 μL) was added to the gel pieces, and the mixture was incubated at 37°C overnight. The supernatant was collected. The gel pieces were washed with 0.1% formic acid in 60% acetonitrile/25 mM ammonium bicarbonate (100 $\mu\text{L} \times 2$). The washes were combined with the supernatants and dried by speed-vac. The dried samples were reconstituted in 0.1% formic acid (15 μL) and then desalted with ZipTip C_{18} column (Millipore #ZTC18S096) by following the manufacturer's instruction.

Mass spectrometry analysis and hit identification: The final desalted samples were analyzed by LC–MS² by using a 75 $\mu\text{m} \times 11$ cm, 15 μm orifice, Luna C_{18} (Phenomenex), 5 μm , 80 \AA LC column and a Thermo Scientific Orbitrap Velos (Rounds 1–4) or Fusion (Round 5) MS system. The MS¹ spectra were collected with an orbitrap detector (at a resolution of 30000), and the MS² spectra were collected with either higher-energy collisional dissociation (HCD) (for rounds 1–3 and 5 at a normalized collision energy of 40.0) or collision-induced dissociation (CID) (for round 4 at a normalized collision energy of 40.0) MS² fragmentation with an orbitrap detector (at a resolution of 7500). The eluent was acetonitrile/ H_2O (0.1% formic acid) with a gradient from 2 to 35% within 1 h at a flow rate of 300 $\mu\text{L min}^{-1}$. The raw peptide data thus collected was searched by Proteome Discoverer with the Sequest algorithm

against UniProt human proteome database to identify protein hits. Default protein grouping was performed, and results were filtered with the following two criteria: 1) "description" field does not contain "keratin"; 2) "score" > 10 by default.

MS-based peptide quantitation: Xcalibur Qual browser was used to view and analyze the raw data from the MS experiments. Exact *m/z* values were calculated for peptides identified with Proteome Discoverer and were used to extract exact mass ion chromatograms from the full MS data. Parameters for peak extraction were as follows: 10 ppm for mass tolerance and Gaussian peak smoothing at 5 points. Integrated peak areas below 50000 were marked as < 50000 based on the detection limit. The peaks thus obtained were confirmed by manually inspecting the retention time, the charge state, and the isotopic pattern.

Cell-cycle analysis: The cell population at different cell-cycle phases was analyzed on the basis of the cellular DNA content by the standard flow cytometry as previously described.^[6a] Briefly, A549 cells were cultured as described above. When cells reached ~70% confluency in a 100 mm cell culture dish, the culture media was replaced by the fresh media containing the corresponding treatment (cells treated with 1% DMSO served as the control). After the specified treatment period, cells were trypsinized and centrifuged with the cell pellet collected. The cell pellet was washed once with PBS and resuspended in PBS (1 mL). To this suspension was added 70% ethanol (9 mL), and the mixture was stored at 4 °C overnight for fixation. Cells were collected by centrifugation, washed twice with PBS, then resuspended in PI staining solution (50 µg mL⁻¹ PI, 200 µg mL⁻¹ RNase A, and 0.1% Triton-X 100 in PBS, 1 mL) and incubated for 30 min at room temperature in the dark. DNA content was quantified with a BD FACSCalibur flow cytometer by using a blue laser ($\lambda=488$ nm) and a long-pass filter ($\lambda=600$ nm) to determine the cell population in the G₀/G₁, S, or G₂/M phase.

Notes

The authors declare no competing financial interest.

Acknowledgements

This research was funded through grants from the US National Institutes of Health National Cancer Institute (NCI) (R01-CA163864 to C.X.), the China Scholarship Council's PhD Abroad Training Plan (201206580001 to C.Z.), and the National Natural Science Foundation of China (81502978 to C.Z.). Mass spectrometry was performed in the Analytical Biochemistry Shared Resource at the Masonic Cancer Center, partially supported by grant P30-CA-077598 from the NCI. We thank Dr. Susith Wickramaratne for help with MS experiments and Paul Champoux for help with flow cytometry.

Keywords: chalcones • chemical probes • cytotoxicity • photoaffinity labeling • tubulin

- [1] a) N. K. Sahu, S. S. Balbhadra, J. Choudhary, D. V. Kohli, *Curr. Med. Chem.* **2012**, *19*, 209–225; b) D. I. Batovska, I. T. Todorova, *Curr. Clin. Pharmacol.* **2010**, *5*, 1–29; c) P. Singh, A. Anand, V. Kumar, *Eur. J. Med. Chem.* **2014**, *85*, 758–777.
- [2] a) B. Zhou, C. Xing, *Med. Chem.* **2015**, *5*, 388–404; b) D. K. Mahapatra, V. Asati, S. K. Bharti, *Eur. J. Med. Chem.* **2015**, *92*, 839–865; c) D. K. Mahapatra, S. K. Bharti, V. Asati, *Eur. J. Med. Chem.* **2015**, *98*, 69–114; d) D. K. Mahapatra, S. K. Bharti, V. Asati, *Eur. J. Med. Chem.* **2015**, *101*, 496–524.
- [3] a) M. L. Go, X. Wu, X. L. Liu, *Curr. Med. Chem.* **2005**, *12*, 483–499; b) S. Vogel, S. Ohmayer, G. Brunner, J. Heilmann, *Bioorg. Med. Chem.* **2008**, *16*, 4286–4293; c) M. M. Rafi, R. T. Rosen, A. Vassil, C. T. Ho, H. Zhang, G. Ghai, G. Lambert, R. S. DiPaola, *Anticancer Res.* **2000**, *20*, 2653–2658; d) S. Vogel, J. Heilmann, *J. Nat. Prod.* **2008**, *71*, 1237–1241; e) D. Wang, H. K. Wong, Y. B. Feng, Z. J. Zhang, *J. Pharm. Pharmacol.* **2014**, *66*, 408–417; f) Y. K. Rao, T. Y. Kao, J. L. Ko, Y. M. Tzeng, *Bioorg. Med. Chem. Lett.* **2010**, *20*, 6508–6512.
- [4] a) W. He, Q. Wang, B. Srinivasan, J. Xu, M. T. Padilla, Z. Li, X. Wang, Y. Liu, X. Gou, H. M. Shen, C. Xing, Y. Lin, *Oncogene* **2014**, *33*, 3004–3013; b) Y. Zhang, B. Srinivasan, C. Xing, J. Lü, *Anticancer Res.* **2012**, *32*, 3689–3698; c) B. Srinivasan, T. E. Johnson, R. Lad, C. Xing, *J. Med. Chem.* **2009**, *52*, 7228–7235.
- [5] a) S. Ducki, R. Forrest, J. A. Hadfield, A. Kendall, N. J. Lawrence, A. T. McGown, D. Rennison, *Bioorg. Med. Chem. Lett.* **1998**, *8*, 1051–1056; b) Y. K. Rao, S. H. Fang, Y. M. Tzeng, *Bioorg. Med. Chem.* **2009**, *17*, 7909–7914.
- [6] a) D. Cao, X. Han, G. Wang, Z. Yang, F. Peng, L. Ma, R. Zhang, H. Ye, M. Tang, W. Wu, K. Lei, J. Wen, J. Chen, J. Qiu, X. Liang, Y. Ran, Y. Sang, M. Xiang, A. Peng, L. Chen, *Eur. J. Med. Chem.* **2013**, *62*, 579–589; b) G. Wang, F. Peng, D. Cao, Z. Yang, X. Han, J. Liu, W. Wu, L. He, L. Ma, J. Chen, Y. Sang, M. Xiang, A. Peng, Y. Wei, L. Chen, *Bioorg. Med. Chem.* **2013**, *21*, 6844–6854; c) C. Zhu, Y. Zuo, R. Wang, B. Liang, X. Yue, G. Wen, N. Shang, L. Huang, Y. Chen, J. Du, X. Bu, *J. Med. Chem.* **2014**, *57*, 6364–6382; d) A. Kamal, A. Mallareddy, P. Suresh, T. B. Shaik, V. Lakshma Nayak, C. Kishor, R. V. Shetti, N. Sankara Rao, J. R. Tamboli, S. Ramakrishna, A. Addlagatta, *Bioorg. Med. Chem.* **2012**, *20*, 3480–3492; e) V. Martel-Frchet, M. Keramidias, A. Nurisso, S. DeBonis, C. Rome, J. L. Coll, A. Boumendjel, D. A. Skoufias, X. Ronot, *Oncotarget* **2015**, *6*, 14669–14686.
- [7] a) K. B. Harikumar, A. B. Kunnumakkara, K. S. Ahn, P. Anand, S. Krishnan, S. Guha, B. B. Aggarwal, *Blood* **2009**, *113*, 2003–2013; b) P. Lorenzo, R. Alvarez, M. A. Ortiz, S. Alvarez, F. J. Piedrafita, A. R. de Lera, *J. Med. Chem.* **2008**, *51*, 5431–5440; c) S. K. Jung, M. H. Lee, D. Y. Lim, J. E. Kim, P. Singh, S. Y. Lee, C. H. Jeong, T. G. Lim, H. Chen, Y. I. Chi, J. K. Kundu, N. H. Lee, C. C. Lee, Y. Y. Cho, A. M. Bode, K. W. Lee, Z. Dong, *J. Biol. Chem.* **2014**, *289*, 35839–35848; d) C. Limper, Y. Wang, S. Ruhl, Z. Wang, Y. Lou, F. Totzke, M. H. Kubbutat, Y. Chovolou, P. Proksch, W. Watjen, *J. Pharm. Pharmacol.* **2013**, *65*, 1393–1408; e) E. B. Yang, K. Zhang, L. Y. Cheng, P. Mack, *Biochem. Biophys. Res. Commun.* **1998**, *245*, 435–438.
- [8] a) S. D. Ramalho, A. Bernades, G. Demetrius, C. Noda-Perez, P. C. Vieira, C. Y. Dos Santos, J. A. da Silva, M. O. de Moraes, K. C. Mousinho, *Chem. Biodiversity* **2013**, *10*, 1999–2006; b) S. H. Kim, E. Lee, K. H. Baek, H. B. Kwon, H. Woo, E. S. Lee, Y. Kwon, Y. Na, *Bioorg. Med. Chem. Lett.* **2013**, *23*, 3320–3324.
- [9] Y. Na, J. M. Nam, *Bioorg. Med. Chem. Lett.* **2011**, *21*, 211–214.
- [10] a) R. Stoll, C. Renner, S. Hansen, S. Palme, C. Klein, A. Belling, W. Zeslawski, M. Kamionka, T. Rehm, P. Muhlhahn, R. Schumacher, F. Hesse, B. Kaluza, W. Voelter, R. A. Engh, T. A. Holak, *Biochemistry* **2001**, *40*, 336–344; b) M. Leão, J. Soares, S. Gomes, L. Raimundo, H. Ramos, C. Bessa, G. Queiroz, S. Domingos, M. Pinto, A. Inga, H. Cidade, L. Saraiva, *Life Sci.* **2015**, *142*, 60–65.
- [11] a) R. Monteiro, A. Faria, I. Azevedo, C. Calhau, *J. Steroid Biochem. Mol. Biol.* **2007**, *105*, 124–130; b) T. Kahyo, S. Ichikawa, T. Hatanaka, M. K. Yamada, M. Setou, *J. Pharmacol. Sci.* **2008**, *108*, 364–371; c) B. Orlikova, M. Schnekenburger, M. Zloh, F. Golais, M. Diederich, D. Tasdemir, *Oncol. Rep.* **2012**, *28*, 797–805; d) B. Zhang, D. Duan, C. Ge, J. Yao, Y. Liu, X. Li, J. Fang, *J. Med. Chem.* **2015**, *58*, 1795–1805; e) J. Zhang, F. J. Ji, Y. Gu, X. Y. Zhang, S. X. Qiao, *Pharmacol. Rep.* **2014**, *66*, 515–519.
- [12] H. Bowne-Anderson, A. Hibbel, J. Howard, *Trends Cell Biol.* **2015**, *25*, 769–779.
- [13] a) J. Sumranjit, S. J. Chung, *Molecules* **2013**, *18*, 10425–10451; b) P. P. Geurink, L. M. Prely, G. A. van der Marel, R. Bischoff, H. S. Overkleeft, *Top. Curr. Chem.* **2012**, *324*, 85–113; c) D. J. Lapinsky, *Bioorg. Med. Chem.* **2012**, *20*, 6237–6247; d) E. Smith, I. Collins, *Future Med. Chem.* **2015**, *7*, 159–183.
- [14] a) C. Hu, D. Nikolic, A. L. Eggler, A. D. Mesezar, R. B. van Breemen, *Anal. Biochem.* **2012**, *421*, 108–114; b) D. J. Wallock-Richards, J. Marles-

- Wright, D. J. Clarke, A. Maitra, M. Dodds, B. Hanley, D. J. Campopiano, *Chem. Commun.* **2015**, 51, 10483–10485.
- [15] J. P. Schülke, L. A. McAllister, K. F. Geoghegan, V. Parikh, T. A. Chappie, P. R. Verhoest, C. J. Schmidt, D. S. Johnson, N. J. Brandon, *ACS Chem. Biol.* **2014**, 9, 2823–2832.
- [16] a) C. J. Schweitzer, T. Jagadish, N. Haverland, P. Ciborowski, M. Belshan, *J. Proteome Res.* **2013**, 12, 559–572; b) C. Tu, Q. Sheng, J. Li, D. Ma, X. Shen, X. Wang, Y. Shyr, Z. Yi, J. Qu, *J. Proteome Res.* **2015**, 14, 4662–4673.
- [17] R. B. Ravelli, B. Gigant, P. A. Curmi, I. Jourdain, S. Lachkar, A. Sobel, M. Knossow, *Nature* **2004**, 428, 198–202.
- [18] a) A. S. Dabert-Gay, B. Czarny, L. Devel, F. Beau, E. Lajeunesse, S. Bregant, R. Thai, A. Yiotakis, V. Dive, *J. Biol. Chem.* **2008**, 283, 31058–31067; b) B. He, S. Velaparthi, G. Pieffet, C. Pennington, A. Mahesh, D. L. Holzle, M. Brunsteiner, R. van Breemen, S. Y. Blond, P. A. Petukhov, *J. Med. Chem.* **2009**, 52, 7003–7013.
- [19] D. Cretu, I. Prassas, P. Saraon, I. Batruch, R. Gandhi, E. P. Diamandis, V. Chandran, *Clin. Proteomics* **2014**, 11, 27.
- [20] a) T. L. Nguyen, C. McGrath, A. R. Hermone, J. C. Burnett, D. W. Zaharevitz, B. W. Day, P. Wipf, E. Hamel, R. Gussio, *J. Med. Chem.* **2005**, 48, 6107–6116; b) M. T. Konieczny, A. Buakowska, D. Pirska, W. Konieczny, A. Skladanowski, M. Sabisz, M. Wojciechowski, K. Lemke, A. Pieczykolan, W. Strozek, *Eur. J. Med. Chem.* **2015**, 89, 733–742.
- [21] K. H. Shen, J. K. Chang, Y. L. Hsu, P. L. Kuo, *Basic Clin. Pharmacol. Toxicol.* **2007**, 101, 254–261.
- [22] a) U. T. Shankavaram, S. Varma, D. Kane, M. Sunshine, K. K. Chary, W. C. Reinhold, Y. Pommier, J. N. Weinstein, *BMC Genomics* **2009**, 10, 277; b) D. W. Zaharevitz, S. L. Holbeck, C. Bowerman, P. A. Svetlik, *J. Mol. Graphics Modell.* **2002**, 20, 297–303.
- [23] a) A. Jordan, J. A. Hadfield, N. J. Lawrence, A. T. McGown, *Med. Res. Rev.* **1998**, 18, 259–296; b) F. Kozielski, D. A. Skoufias, R. L. Indorato, Y. Saoudi, P. R. Jungblut, H. K. Hustoft, M. Strozynski, B. Thiede, *Proteomics* **2008**, 8, 289–300; c) L. M. MacDonald, A. Armson, A. R. Thompson, J. A. Reynoldson, *Mol. Biochem. Parasitol.* **2004**, 138, 89–96; d) J. H. Wei, J. Seemann, *Mol. Cancer Ther.* **2010**, 9, 3375–3385.

Received: March 11, 2016

Revised: April 12, 2016

Published online on ■■■■■, 0000

FULL PAPERS

Best PALs: A photoaffinity labeling approach was used to search for the direct cellular target responsible for the cytotoxicity of chalcone in a whole-cell-based assay. β -Tubulin was unambiguously revealed by mass spectrometric analysis to be this target. Evidence suggests that the potential binding site of chalcones on β -tubulin is the colchicine binding site.



B. Zhou, X. Yu, C. Zhuang,* P. Villalta,
Y. Lin, J. Lu, C. Xing*

Unambiguous Identification of β -Tubulin as the Direct Cellular Target Responsible for the Cytotoxicity of Chalcone by Photoaffinity Labeling

